Bioorganic & Medicinal Chemistry Letters 21 (2011) 1206–1213

Contents lists available at ScienceDirect

Bioorganic & Medicinal Chemistry Letters

journal homepage: www.elsevier.com/locate/bmcl

Conformationally constrained farnesoid X receptor (FXR) agonists: Heteroaryl replacements of the naphthalene

Jonathan Y. Bass [a,†], Justin A. Caravella [b,‡], Lihong Chen [c], Katrina L. Creech [d], David N. Deaton [a,*], Kevin P. Madauss [b], Harry B. Marr [e], Robert B. McFadyen [a], Aaron B. Miller [b], Wendy Y. Mills [a,§], Frank Navas III [a,¶], Derek J. Parks [f], Terrence L. Smalley Jr. [a], Paul K. Spearing [a], Dan Todd [g], Shawn P. Williams [b], G. Bruce Wisely [f]

[a] Department of Medicinal Chemistry, GlaxoSmithKline, Research Triangle Park, NC 27709, USA
[b] Department of Molecular Discovery Research, Computational and Structural Chemistry Research, GlaxoSmithKline, Research Triangle Park, NC 27709, USA
[c] Department of Molecular Pharmacology, GlaxoSmithKline, Research Triangle Park, NC 27709, USA
[d] Department of Molecular Discovery Research, Screening and Compound Profiling, GlaxoSmithKline, Research Triangle Park, NC 27709, USA
[e] Department of Drug Metabolism and Pharmacokinetics, GlaxoSmithKline, Research Triangle Park, NC 27709, USA
[f] Department of Molecular Discovery Research, Biological Reagents and Assay Development, GlaxoSmithKline, Research Triangle Park, NC, 27709, USA
[g] Department of Pharmaceutical Development, Physical Properties and Developability, GlaxoSmithKline, Research Triangle Park, NC 27709, USA

ARTICLE INFO

Article history:
Received 8 October 2010
Revised 15 December 2010
Accepted 16 December 2010
Available online 23 December 2010

Keywords:
Farnesoid X receptor
FXR
Nuclear receptor modulator
FXR X-ray co-crystal structure
GW 4064
GSK8062
Bile acid receptor
NR1H4 GSK2324

ABSTRACT

To improve on the drug properties of GSK8062 **1b**, a series of heteroaryl bicyclic naphthalene replacements were prepared. The quinoline **1c** was an equipotent FXR agonist with improved drug developability parameters relative to **1b**. In addition, analog **1c** lowered body weight gain and serum glucose in a DIO mouse model of diabetes.

Bile acids are synthesized from cholesterol and serve as the primary route of elimination of cholesterol from mammals. Bile acids and their conjugates are amphipathic molecules that can form mixed micelles, facilitating the dissolution and absorption of dietary lipids and fat-soluble vitamins. Since bile acids can disrupt cell bilayers, their concentrations must be tightly controlled and nature has developed several regulatory mechanisms to monitor and adjust bile acid levels.[1,2] These signalling pathways include activation of the c-Jun N-terminal kinase (JNK) pathway[3], signal transduction of the 7-transmembrane receptor family member bile acid receptor TGR5 (GPBAR1, M-BAR)[4], and transcription mediated through the nuclear receptor family member farnesoid X receptor (FXR, NR1H4, bile acid receptor (BAR)).[5]

Besides regulating bile acid homeostasis, FXR also has additional functions in metabolism. FXR is highly expressed in tissues implicated in bile acid recirculation and elimination, including liver, gall bladder, intestine, and kidney, as well as having significant expression in adrenal glands.[6,7] The bile acid chenodeoxycholic acid (CDCA) is the natural ligand with the highest affinity for FXR, with cholic acid (CA), deoxycholic acid (DCA), and lithocholic acid (LCA) also having affinity for the receptor. Coupled to bile acids' roles in the dietary pathway, the signalling mechanisms of these molecules have also evolved to regulate lipid[8–10] and glucose metabolism,[11–13] attenuate intestinal infection,[14–16] assist in xenobiotic elimination,[17] and influence liver regeneration[18] through FXR. With FXR's multiple physiological roles, FXR modulators could be utilized for the treatment of cholestasis,[19–21] liver fibrosis,[22–25] liver cancer,[26,27] steatohepatitis,[28]

* Corresponding author. Tel.: +1 919 483 6270.
E-mail address: david.n.deaton@gsk.com (D.N. Deaton).
† Present address: Department of Chemistry, University of California, Irvine, CA 92697, USA.
‡ Present address: Biogen Idec, 14 Cambridge Center, Cambridge, MA 02142, USA.
§ Present address: United States Army Research Laboratory, Research Triangle Park, NC 27709, USA.
¶ Present Address: Department of Organic and Medicinal Chemistry, Research Triangle Institute, RTP, NC 27709, USA.

0960-894X/$ - see front matter © 2010 Elsevier Ltd. All rights reserved.
doi:10.1016/j.bmcl.2010.12.089

atherosclerosis,[29–32] cholesterol gallstone disease,[33] diabetes,[13] obesity,[34] metabolic syndrome,[35] and inflammatory bowel disease.[14,15]

Employing an iterative combinatorial library synthesis and screening approach versus orphan nuclear receptors, Glaxo Wellcome scientists discovered the potent and selective FXR agonist GW 4064A **1a**.[9] This molecule, along with other FXR ligands[36–40] including 6-ethyl-CDCA[41] and fexaramine,[42] was instrumental in probing the physiological roles of FXR. Recently, Exelixis and Wyeth researchers have reported the discovery of another chemical class of FXR modulators, exemplified by WAY362450 (XL335).[43] Although a potent FXR tool compound, GW 4064 **1a** had several limitations as a drug candidate, including UV light instability, a questionable stilbene pharmacophore, and limited oral bioavailability. Thus, GlaxoSmithKline medicinal chemists sought to improve on this ligand. Structure–activity relationship (SAR) studies of the isoxazole substituents[39] and conformational constraints of the benzoic acid[37] and internal aryl rings[38] led to the identification of GSK8062 **1b** (TT EC_{50} = 68 nM, %Max = 104), a potent FXR agonist with improved light stability, good oral bioavailability in dog and monkey, and an acceptable in vitro safety profile.[37] With the inherent risk associated with drug discovery, a replacement molecule was sought to mitigate development risks in the event that GSK8062 **1b** could not be advanced. In addition to desiring a back-up molecule with the desirable properties of GSK8062 **1b**, GlaxoSmithKline desired a drug candidate that had improvements relative to GSK8062 **1b**. First, the limited aqueous solubility of GSK8062 **1b** at neutral pH values necessitated the use of non-standard formulations to obtain adequate exposure during safety assessment studies. Second, the limited oral exposure of GSK8062 **1b** in rats, resulting from its high clearance, required the use of mice for rodent species safety assessment studies. Mice, because of their size and physiology, are more difficult to correctly dose during safety assessment studies. Third, in an exploratory salt screening study employing frequently used counterions such as sodium or potassium, difficulty was encountered in discovering a suitable crystalline salt version of GSK8062 **1b**, necessitating the use of a less conventional salt version. Thus a follow-on drug candidate was desired with similar/better potency and selectivity for FXR with improved water solubility, better rat pharmacokinetics, and a more conventional solid formulation. Believing that improved aqueous solubility might increase rat exposure, a strategy was devised to replace the naphthyl ring of GSK8062 **1b** with heteroaryl bicyclic systems to improve hydrophilicity.

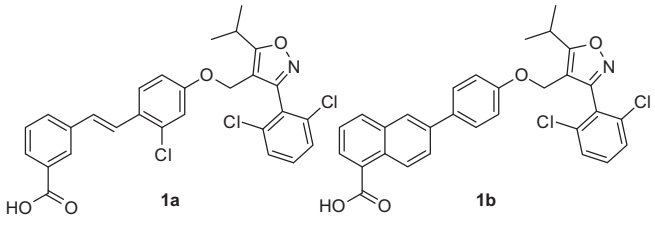

The heteroaryl carboxylic acid analogs **1c**–**1v** were prepared by one of two routes as depicted in Schemes 1 and 2 with the full experimental details provided in the Supplementary data. The quinolines **2a**–**2c**, and **2j**–**2l** and the isoquinoline **2e** were coupled to the appropriate boronates **3a**–**3d**, employing the Suzuki protocol to provide the phenols **4a**–**4h** as shown in Scheme 1. Then, O-alkylation of the phenols **4a**–**4h** with the alkyl chloride **5a**[37] produced aryl ethers, which upon base-catalyzed hydrolysis of the esters afforded the corresponding carboxylic acids **1c**–**1f** and **1k**–**1n**.

Alternatively, palladium-mediated Suzuki coupling of the heteroaryl bromides of the isoquinoline **2f**, quinazoline **2g**, quinoxaline **2h**, 1,2,4-benzotriazene **2i**, or quinolines **2m**–**2s** with the aryl boronate **6a**[44] gave the corresponding biaryl derivatives, whose esters were hydrolyzed in a similar manner to Scheme 1,

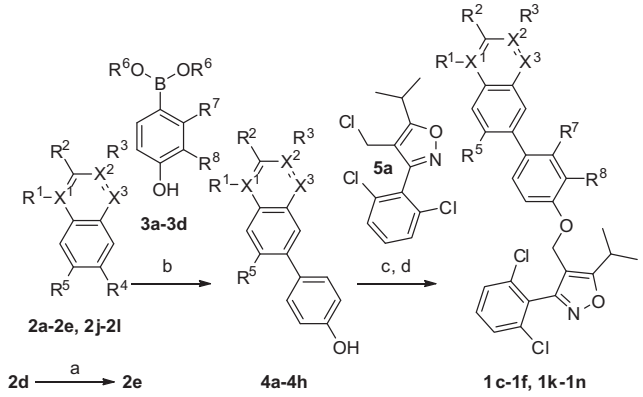

Scheme 1. Reagents and conditions: (a) **2d**, NEt_3, Tf_2O,CH_2Cl_2, (b) **2a**–**2c**, **2e**, or **2j**–**2l**, **3a**–**3d**, Na_2CO_3 or K_3PO_4, $Pd(PPh_3)_4$, or $Pd(OAc)_2$ and PPh_3, DME or dioxane, H_2O, 60–80 °C; $MeSO_3H$, MeOH, ↓↑, 40–98%; (c) **5a**, Cs_2CO_3 or K_2CO_3, DMF, 50–70 °C, 22–70%; (d) NaOH, THF, MeOH or EtOH, H_2O, 25–60 °C or microwave at 90–100 °C, 79–99%.

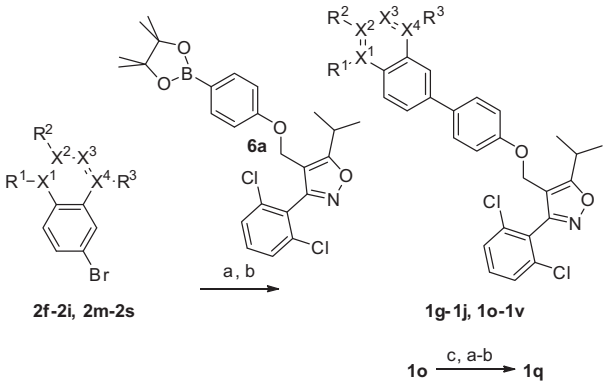

Scheme 2. Reagents and conditions: (a) **2f**–**2i**, or **2m**–**2s**, **6a**, K_3PO_4, $Pd(OAc)_2$ and PPh_3, dioxane, H_2O, 60–80 °C, 22–91%; (b) NaOH, THF, MeOH or EtOH, H_2O, 25–60 °C or microwave at 90–100 °C, 8–99%; (c) **1o**, 2,6-lutidine, DMAP, Tf_2O, $ClCH_2CH_2Cl$, 60 °C, 32%.

to provide the desired carboxylic acids **1g**–**1j**, **1o**–**1p**, and **1r**–**1v** as illustrated in Scheme 2. The carboxylic acid **1q** (R^2 = CO_2H, R^3 = Et) was prepared from the phenol **1o** (R^2 = CO_2Me, R^3 = OH). First, conversion of the phenol to the triflate with trifluoromethanesulfonic anhydride, then Suzuki coupling with ethyl boronic acid, followed by ester hydrolysis yielded the carboxylic acid **1q** (R^2 = CO_2H, R^3 = Et).

Some of the heteroaryl esters, such as the quinolines **2a**, **2c**, and **2m** were commercially available, while others such as quinoline **2b**,[45] and isoquinoline **2d**[46] were known in the literature. The remaining heteroaryl esters were prepared as depicted in Schemes 3–8. The isoquinoline **2f** was prepared from the phenethyl amine **9a** as shown in Scheme 3. Sulfonation of the amine **9a** with benzenesulfonyl chloride, followed by alkylation with the chloride **8a**, prepared from the thioether **7a**, and tin(IV) chloride catalyzed Friedel–Crafts cyclization gave the regioisomeric tetrahydroisoquinolines **10a** and **10b**. Subsequent base catalyzed elimination/aromatization of the desired major product **10b** afforded the isoquinoline **2f**.

The quinazoline **2g** was prepared as shown in Scheme 4. The aniline **11a** was acylated with ethyl chlorooxoacetate to give the amide, which was heated at reflux with ammonium acetate to provide the quinazoline **2g**.

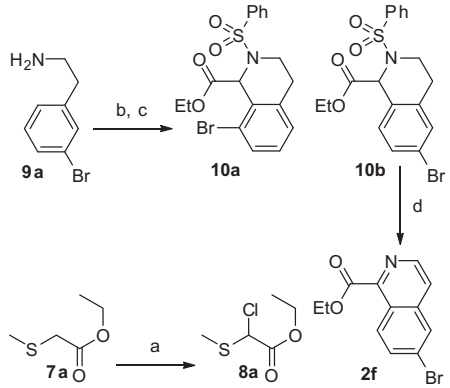

Scheme 3. Reagents and conditions: (a) *N*-chlorosuccinimide, CCl_4, 0–25 °C, 43%; (b) $PhSO_2Cl$, iPr_2NEt, CH_2Cl_2, 0–25 °C, 95%; (c) **8a**, $SnCl_4$, $ClCH_2CH_2Cl$, ↑↓, 79% and 19%; (d) DBU, PhMe, 59%.

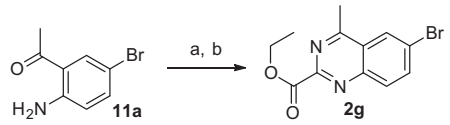

Scheme 4. Reagents and conditions: (a) EtO_2CCOCl, pyridine, CH_2Cl_2, 0–25 °C, 85%; (b) NH_4OAc, HOAc, ↑↓, 49%.

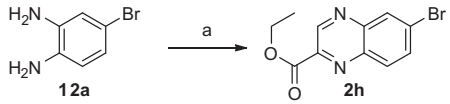

Scheme 5. Reagents and conditions: (a) EtO_2CCOCH_2Br, NMP, 25 °C, 13%.

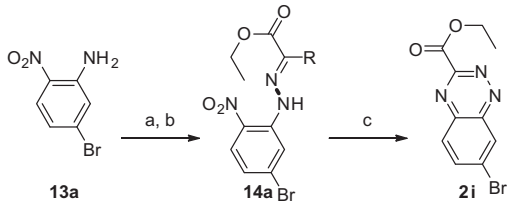

Scheme 6. Reagents and conditions: (a) $NaNO_2$, HCl, MeOH, H_2O; $EtO_2CCHClCOCH_3$, 0–25 °C, 63%; (b) NH_3, dioxane, 25 °C, 83%; (c) Fe, HCl, HOAc, H_2O, 25 °C, 41%.

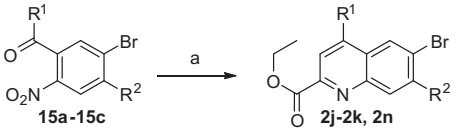

Scheme 7. Reagents and conditions: (a) **15a**–**15c**, $ZnCl_2$, $SnCl_2$, 4Å molecular sieves, $CH_3CH_2COCO_2Et$ or CH_3COCO_2Et, EtOH, 70 °C, 3–20%.

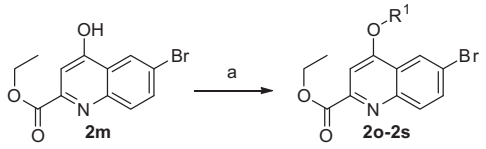

Scheme 8. Reagents and conditions: (a) Ag_2CO_3, R^1I, THF, 33–57%.

The quinoxaline **2h** was synthesized as illustrated in Scheme 5. Alkylation of the diamine **12a** with ethyl bromopyruvate, followed by intramolecular condensation yielded the quinoxaline **2h**.

The 1,2,4-benzotriazene **2i** was synthesized as depicted in Scheme 6. The aniline **13a** was diazotized, followed by trapping with ethyl 2-chloroacetoacetate to give the hydrazonoyl chloride **14a** (R = Cl). Then, displacement of the chloride with ammonia afforded the imidohydrazide **14a** (R = NH_2). Reduction of the nitro moiety and cyclization then provided the desired 1,2,4-benzotriazene **2i**.

The quinolines **2j**, **2k**, and **2n** were prepared as shown in Scheme 7. One pot in situ tin(II) chloride reduction of the nitroarenes **15a**–**15c**, followed by zinc(II) chloride catalyzed imine formation with ethyl pyruvate or ethyl 2-oxobutanoate, and cyclization provided the quinolines **2j**, **2k**, and **2n**.

The quinolines **2o**–**2s** were prepared as shown in Scheme 8. Silver carbonate catalyzed alkylation of phenol **2m** with various alkyl iodides yielded the desired quinolines **2o**–**2s**.

The structure–activity relationships of the heteroaryl bicyclic analogs are depicted in Table 1. Knowing from the FXR/GSK8062 **1b** X-ray co-crystal structure[37] that the carboxylic acid moiety was near the solvent front, analogs that insert a nitrogen atom in the proximal ring of the naphthalene might be permissible with minimal desolvation cost. Also, since the naphthyl analogs, exemplified by **1b**, tolerated both α- (TT EC_{50} = 68 nM) and β-carboxylic acids (TT EC_{50} = 45 nM),[37] proximal aza-analogs were prepared with the acid functionality at either position of the ring.

As exemplified by the quinoline **1c** (TT EC_{50} = 50 nM) and isoquinoline **1f** (TT EC_{50} = 77 nM), the nitrogen atom was well tolerated at the 1- and 3-positions of the aza-naphthalene template, as these analogs have similar potency in both the fluorescent resonance energy transfer (FRET) assay for recruitment of the co-activator peptide of SRC-1 and the transient transfection (TT) assay for induction of a luciferase reporter gene. Both quinoline **1c** (TT %Max = 102) and isoquinoline **1f** (TT %Max = 86) are full FXR agonists in these assays. Thus, either the cost to desolvate the additional nitrogen atom of these analogs must be small, or the lone pair on the nitrogen atom participates in a direct or water bridging (vide infra) hydrogen bond to the protein, where the binding energy from this putative hydrogen bond helps compensate for the desolvation cost.

In contrast, the nitrogen atom was less well accommodated at the 2- and 4-positions of the aza-naphthalene template as shown by quinolines **1d** (TT EC_{50} = 560 nM) and **1e** (TT EC_{50} = 260 nM) and isoquinoline **1g** (TT EC_{50} = 190 nM), which, although full agonists, exhibit diminished potency relative to their corresponding naphthyl analogs. In addition to the desolvation cost, inferences from X-ray structures[37] suggest that the 4-aza analogs **1d** and **1e** place the nitrogen lone pair near a hydrophobic part of the protein, which is probably detrimental to binding. The carboxylic acids of quinoline **1c** and isoquinoline **1f** prefer a planar conformation that maximizes aryl and carbonyl π-bond resonance energy stabilization and allows an intramolecular hydrogen bond between the carboxylic acid and the ring nitrogen. In contrast, the 2-aza analog **1g** likely has its carboxylic acid moiety twisted out of plain, similar to the carboxylic acid of GSK8062 **1b** in its X-ray co-crystal structure,[37] to avoid a *syn*-pentane interaction with the 8-hydrogen. The lack of this intramolecular hydrogen bond likely leads to stronger solvation of the isoquinoline nitrogen of **1g**. Thus, a higher desolvation penalty may result upon binding, leading to reduced potency for isoquinoline **1g**.

Inserting more than one nitrogen into the naphthalene template, as in the quinazoline **1h** (TT EC_{50} = 1000 nM), the quinoxaline **1i** (TT EC_{50} = 690 nM), or the 1,2,4-benzotriazine **1j** (TT EC_{50} = >10,000 nM), resulted in a significant decrease in transient transfection potency. Since activity in the cell free FRET assay was maintained, the decrease in the TT assay may reflect limited cell penetration in this assay. Alternatively, the African green monkey CV-1 cells used in the TT assay likely contain additional coactivators and corepressors besides SRC-1, which may alter potency/efficacy relative to the cell free FRET assay.

Table 1
Activation of human FXR

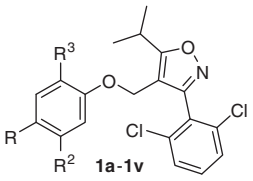

1a-1v

#	R	R^1	FXR FRET EC_{50} nM[a] (%Max[b])	FXR TT EC_{50} nM[c] (%Max[b])
1a	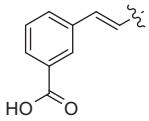	R^2 = H R^3 = H	59 (100)	65 (100)
1b	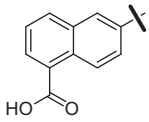	R^2 = H R^3 = H	87 (134)	68 (104)
1c	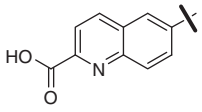	R^2 = H R^3 = H	120 (105)	50 (102)
1d	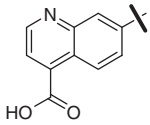	R^2 = H R^3 = H	340 (99)	560 (85)
1e	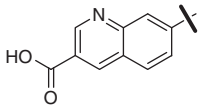	R^2 = H R^3 = H	200 (87)	260 (88)
1f	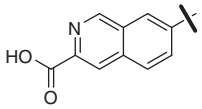	R^2 = H R^3 = H	120 (83)	77 (86)
1g	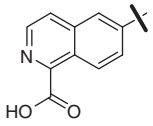	R^2 = H R^3 = H	380 (92)	190 (102)
1h	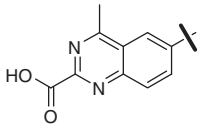	R^2 = H R^3 = H	140 (102)	1000 (127)
1i	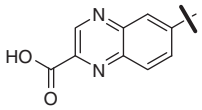	R^2 = H R^3 = H	150 (96)	690 (109)
1j	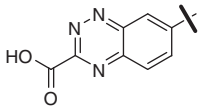	R^2 = H R^3 = H	360 (100)	>10,000 (—)
1k	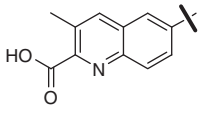	R^2 = H R^3 = H	140 (107)	38 (101)
1l	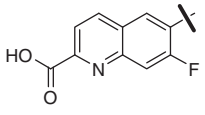	R^2 = H R^3 = H	240 (115)	110 (107)

(*continued on next page*)

Table 1 (*continued*)

#	R	R^1	FXR FRET EC_{50} nM[a] (%Max[b])	FXR TT EC_{50} nM[c] (%Max[b])
1m	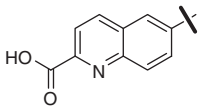	R^2 = Me R^3 = H	250 (87)	52 (91)
1n	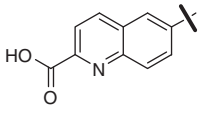	R^2 = H R^3 = Me	110 (100)	44 (94)
1o	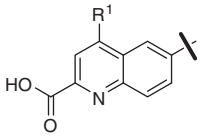	R^1 = OH R^2 = H R^3 = H	51 (91)	>10,000 (—)
1p	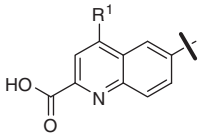	R^1 = Me R^2 = H R^3 = H	81 (108)	24 (107)
1q	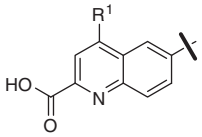	R^1 = Et R^2 = H R^3 = H	75 (106)	32 (109)
1r	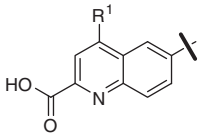	R^1 = OMe R^2 = H R^3 = H	58 (113)	17 (107)
1s	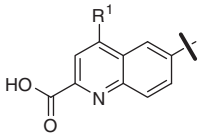	R^1 = OEt R^2 = H R^3 = H	52 (99)	14 (84)
1t	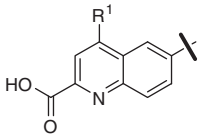	R^1 = OiPr R^2 = H R^3 = H	40 (113)	14 (103)
1u	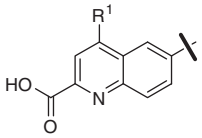	R^1 = OnPr R^2 = H R^3 = H	59 (113)	22 (93)
1v	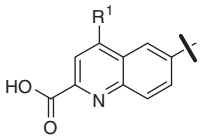	R^1 = OiBu R^2 = H R^3 = H	78 (105)	81 (93)

[a] FXR ligand seeking assay measuring ligand-mediated interaction of the SRC-1 peptide (B-CPSSHSSLTERHKILHRLLQEGSPS-$CONH_2$) with the FXR $^{237–472}$LBD, using 5 nM biotinylated human FXR LBD coupled to 5 nM allophycocyanin-labeled streptavidin and 10 nM biotinylated human SRC-1 coupled to 5 nM Europium-labeled streptavidin as reagents in 10 mM DTT, 0.1 g/L BSA, 50 mM NaF, 50 mM MOPS, 1 mM EDTA, and 50 μM CHAPS, at pH 7.5. The EC_{50} values are the mean of at least two assays.

[b] Maximum percent efficacy of the test compound relative to FXR activation via GW 4064 **1a**.

[c] FXR transient transfection assay measuring the ligand-mediated luminescence resulting from FXR-induced transcription of a luciferase reporter. FXR and the luciferase reporter genes are transfected into African green monkey CV-1 kidney cells, then treated with test compound. The EC_{50} values are the mean of at least two assays.

The effect of substitution on the potency/efficacy of the azanaphthalenes was also explored. The 3-methyl group of quinoline **1k** should force the carboxylic acid to twist out of plane to avoid a *syn*-pentane interaction, possibly enhancing its interaction with the guanidine moiety of ^{331}Arg, while maybe increasing the desolvation cost of the quinoline nitrogen due to the loss of the internal hydrogen bond. Quinoline **1k** (TT EC_{50} = 38 nM) exhibited similar potency as **1c**, suggesting that any gain from a stronger interaction with ^{331}Arg was likely offset by a larger desolvation cost.

Although small in size, the 3-fluoro group of quinoline **1l** (TT EC_{50} = 110 nM) could alter the rotamer conformation between the quinoline and aryl rings affecting receptor binding, yet the drop

in potency was negligible. Similarly, the 2-methyl substituent on the phenyl ring of quinoline **1m** (TT EC_{50} = 52 nM) could also alter rotamer population energies between the quinoline and aryl rings, but had no effect on receptor potency relative to **1c**. Furthermore, substitution at the 3-position of the phenyl ring with a methyl group, as in quinoline **1n** (TT EC_{50} = 44 nM), also maintained receptor affinity, despite potentially affecting the conformation of the oxymethylene linker. Likely, in these three cases, the receptor could tolerate the added substituent with minimal changes in conformation.

Similar to the 1,2,4-benzotriazine **1j**, the 4-hydroxyquinoline **1o** (TT EC_{50} = >10,000 nM) was inactive in the transient transfection assay, but exhibited good potency in the cell free FRET assay (FRET EC_{50} = 51 nM), suggesting poor cell permeability. In contrast, 4-alkyl- and 4-alkoxy-substituents, exemplified by quinolines **1p**–**1v**, were active in the whole cell TT assay. The methylquinoline **1p** (TT EC_{50} = 24 nM), the ethylquinoline **1q** (TT EC_{50} = 32 nM), the methoxyquinoline **1r** (TT EC_{50} = 17 nM) and the *n*-propoxyquinoline **1u** (TT EC_{50} = 22 nM) were potent, full FXR agonists. Whereas, the ethoxyquinoline **1s** (TT EC_{50} = 14 nM) and the *iso*-propoxyquinoline **1t** (TT EC_{50} = 14 nM) appeared to be optimal ligands and were modestly more potent than starting quinoline **1c**, the *iso*-butoxyquinoline **1v** (TT EC_{50} = 81 nM) was less potent and its substituent might be approaching the limit of accommodation by the protein. The X-ray co-crystal structure of GSK8062 **1b**[37] shows that this region of the receptor is hydrophobic, and contains little room for 4-position substitution on the agonist. Clearly, the ligand binding domain is capable of moving to allow binding by these analogs. Although these 4-substituted analogs resulted in modest gains in potency, they came at the cost of reduced water solubility.

The X-ray co-crystal structures of quinoline **1c** and isoquinoline **1f** with FXR were obtained and are depicted in Figures 1 and 2. They further reinforce the receptor recognition elements necessary for FXR gene transcription in this chemical series. In both structures, the isoxazole resides adjacent to ^{454}Trp and ^{447}His on the C-terminal end of helix 10, with ^{469}Trp located on activation function 2 region (helix 12), making an edge to face stacking interaction with the isoxazole. Further stabilization of the active protein conformer for recruitment of co-activator proteins for gene transcription is provided by the *iso*-propyl group, which occupies a pocket formed by ^{284}Phe, ^{287}Leu, ^{454}Trp, and ^{461}Phe. In addition, the di-*ortho* substitution on the 2,6-dichlorophenyl ring makes the aryl ring's lowest energy conformation the rotamer that is orthogonal to the isoxazole ring, minimizing entropic loss upon binding, while maximizing enthalpic interactions with the ligand binding domain in this region of the protein. While the above interactions are likely crucial to stabilize the hydrophobic core of the receptor, leading to an active conformation of the receptor capable of shedding co-repressors and recruiting co-activators to induce gene transcription, the phenyl scaffold connecting the isoxazole to the heteroaryl bicycle is probably enhancing potency via hydrophobic interactions with the receptor, as well as orienting the two terminal pharmacophores for optimal interactions with the protein.

In both structures, the carboxylic acids are co-planar with their heteroaryl ring, similar to the GW 4064 **1a** X-ray co-crystal structure,[37] but in contrast to the GSK8062 **1b** X-ray co-crystal structure in which the carboxylic acid is orthogonal to the naphthalene ring, as shown in Figure 1. In both the quinoline **1c** and the isoquinoline **1f** X-ray cocrystal structures, one NH_2 of the guanidine group of ^{331}Arg on helix 5 of FXR forms electrostatic interactions with one of the oxygen atoms of the respective carboxylic acids. In addition to hydrophobic contacts with the protein, the quinoline nitrogen of agonist **1c** forms a water-mediated hydrogen bond with the same NH_2 that interacts with the quinoline carboxylate as well as with the ε-NH of ^{331}Arg's guanidine. Although the planar interaction of the acid moiety is probably less favored than the orthogonal

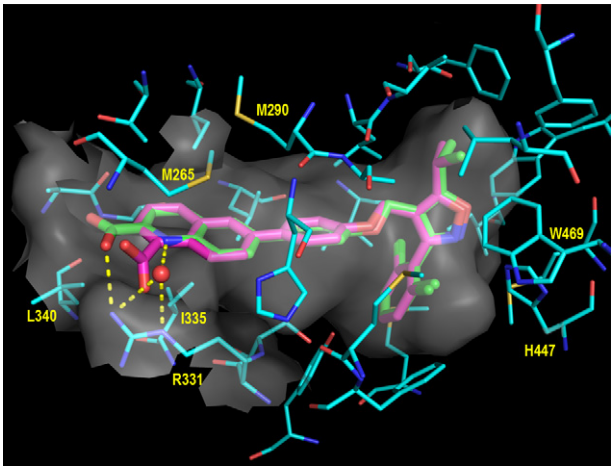

Figure 1. Ligand binding domain of the X-ray co-crystal structure of quinoline **1c** (ligand **1c** carbons colored green) complexed with FXR. The FXR carbons from the co-crystal structure with **1c** are colored cyan. The semi-transparent grey surface represents the molecular surface, while hydrogen bonds are depicted as yellow dashed lines. GSK8062 **1b** (ligand **1b** carbons colored magenta) has been superimposed into this structure based on its published X-ray co-crystal structure. The coordinates have been deposited in the Brookhaven Protein Data Bank (**1b** PDB code 3DCU, **1c** PDB Code 3P89). This figure was generated using PYMOL version 1.3 (www.pymol.org).

interaction of the GSK8062 **1b** structure, the through water hydrogen bond between the quinoline nitrogen and the side chain of ^{331}Arg likely offsets any reduced binding energy between the acid and the guanidine.

As shown in Figure 2, in the isoquinoline **1f** X-ray co-crystal structure, the isoquinoline ring is rotated 180° relative to the quinoline ring of agonist **1c**, while the carboxylic acids are only slightly shifted, maintaining the electrostatic interaction with ^{331}Arg. This places the isoquinoline nitrogen of **1f** in a relatively similar position as the quinoline nitrogen of **1c**. Although no water mediated hydrogen bond to the guanidine of ^{331}Arg was detected in this lower resolution structure (**1f** 2.7 Å versus **1c** 2.35 Å), one might infer that

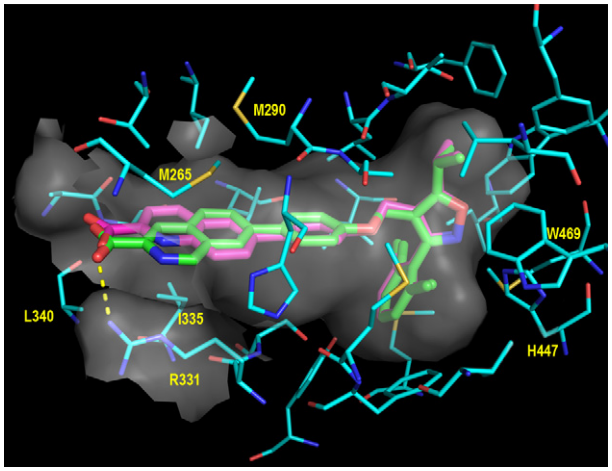

Figure 2. Ligand binding domain of the X-ray co-crystal structure of isoquinoline **1f** (ligand **1f** carbons colored green) complexed with FXR. The FXR carbons from the co-crystal structure with **1f** are colored cyan. The semi-transparent grey surface represents the molecular surface, while hydrogen bonds are depicted as yellow dashed lines. Quinoline **1c** (ligand **1c** carbons colored magenta) has been superimposed into this structure based on its X-ray co-crystal structure above. The coordinates have been deposited in the Brookhaven Protein Data Bank (**1c** PDB code 3P89, **1f** PDB Code 3P88). This figure was generated using PYMOL version 1.3 (www.pymol.org).

Table 2
Pharmacokinetics of FXR agonists

#	Species	$t_{1/2}$[a] (min)	C_l[b] (mL/min/kg)	V_{SS}[c] (mL/kg)	F[d] (%)	DNAUC[e] (ng h kg/mL mg)
1c	Mouse	84	23	1600	42	310
	Rat	170	32	3400	23	130
	Beagle	110	4.4	310	23	1260
	Cyno	120	3.1	150	15	850
1f	Mouse	250	29	5100	6.3	36
	Rat	88	18	1800	30	300
	Beagle	230	8.2	2000	15	320
	Cyno	620	11	3100	2.5	40

[a] $t_{1/2}$ is the iv terminal half-life dosed as a solution. All in vivo pharmacokinetic values are the mean at least two experiments.
[b] C_l is the iv total clearance.
[c] V_{SS} is the iv steady state volume of distribution.
[d] F is the oral bioavailability dosed as a solution.
[e] DNAUC is the oral dose normalized area under the curve.

Table 3
Diet-induced obese mouse study—body weight (g)[a]

Diet Treatment	NC[b] Vehicle	HFD[c] Vehicle	HFD[c] 10 mg/kg	HFD[c] 30 mg/kg	HFD[c] 100 mg/kg
Baseline	26.7 ± 0.4[e]	30.3 ± 0.6	30.0 ± 0.8	29.6 ± 0.9	29.1 ± 0.8
Week 1	26.8 ± 0.4[d]	29.5 ± 0.5	29.4 ± 0.7	28.4 ± 0.8	25.6 ± 0.4[f]
Week 2	26.1 ± 0.4[f]	29.6 ± 0.4	29.3 ± 0.6	27.8 ± 0.7	23.2 ± 0.5[f]
Week 3	25.7 ± 0.4[f]	30.0 ± 0.5	29.0 ± 0.6	27.5 ± 0.7[d]	24.1 ± 0.7[f]
Week 4	26.2 ± 0.5[e]	29.7 ± 0.6	29.0 ± 0.7	27.3 ± 0.6	25.6 ± 0.6[f]

[a] The results are presented as mean ± SEM and analyzed by one-way ANOVA followed by the Tukey's honest significance test.
[b] NC = normal chow diet.
[c] HFD = high fat diet.
[d] p <0.05 versus the high fat diet group.
[e] p <0.01 versus the high fat diet group.
[f] p <0.001 versus the high fat diet group.

this ring flip occurred to allow a similar through water interaction with the receptor. Alternatively, or in addition, the ring might have flipped to keep the isoquinoline nitrogen away from a hydrophobic area formed by the side chains of ^{270}Thr, ^{273}Ile, ^{335}Ile, ^{343}Gly, and ^{348}Leu. In this structure, small rotamer changes in the alkyl chains of ^{335}Ile and ^{450}Met in the ligand binding domain of FXR are evident, although little difference is observed between the quinoline **1c** and isoquinoline **1f** conformations in those regions of the molecules. Finally, the ^{340}Leu *iso*-butyl group is visible in the higher resolution structure of quinoline **1c** but not in the isoquinoline **1f** structure.

As shown in Table 2, quinoline **1c** and isoquinoline **1f** were profiled in four species to ascertain their pharmacokinetic parameters. Quinoline **1c** had low clearances in the mouse, beagle dog, and cynomolgus monkey, with a medium clearance in the Sprague–Dawley rat, while isoquinoline **1f** had low clearances in the rat and dog, with medium clearances in the mouse and monkey. Although the clearance for quinoline **1c** was higher in the rat, its corresponding higher volume of distribution resulted in a longer terminal half-life than in the other species due to their lower volumes of distribution. Quinoline **1c** had a good oral bioavailability in the mouse, which decreased in higher species progressively to an oral bioavailability of 15% in the monkey. This class of compounds exhibits high liver to plasma ratios, thus high first pass clearances may be limiting oral bioavailabilities.[36] Isoquinoline **1f** generally exhibited higher volumes than quinoline **1c**, resulting in longer terminal half-lives, but its decreased oral bioavailabilities and po dose-normalized areas under the curve precluded it from further development.

Quinoline **1c** compared favorably to GSK8062 **1b** in its pharmacokinetic parameters,[37] with a similar oral dose normalized area under the curve in monkey (**1b** DNAUC = 1130 ng h kg/mL mg vs **1c** DNAUC = 850 ng h kg/mL mg) and a 5-fold better oral exposure in the rat (**1b** DNAUC = 23 ng h kg/mL mg vs **1c** DNAUC = 130 ng h kg/mL mg). Furthermore, quinoline **1c**'s Cyp 450 inhibition profile in pooled human liver microsomal assays was reasonable (1A2 IC_{50} = 21,000 nM, 2C9 IC_{50} = 4400 nM, 2C19 IC_{50} = >33,000 nM, 2D6 IC_{50} = >33,000 nM, 3A4 [midazolam] IC_{50} = >33,000 nM, 3A4 [atorvastatin] IC_{50} = 5100 nM, 3A4 [nifedipine] IC_{50} = 11,000 nM). Similar to GSK8062 **1b**, quinoline **1c** was at least 100-fold selective for FXR versus a panel of closely homologous nuclear receptors, consisting of LRH, LXRα, LXRβ, PPARα, PPARγ, PPARδ, PXR, RORα, and RXRα. Also, quinoline **1c** was highly permeable in the Madin–Darby canine kidney cell (MDCK) absorption assay[47] with an apparent permeability factor P_{APP} = 183 nm/s. In contrast to GSK8062 **1b** (sol. = 1 ng/mL), quinoline **1c** was 60 times more soluble in fasted state-simulated intestinal fluid (FaS-SIF) at pH 6.5 (sol. = 60 ng/mL). The enhanced solubility of quinoline **1c** allowed a simple pH buffered water formulation to be utilized for safety assessment dosing. Furthermore, a suitable crystalline potassium salt of quinoline **1c** was discovered. Also, with the lower clearance of quinoline **1c** in rats, resulting in better oral exposure, the rat could be employed

Table 4
Diet-induced obese mouse study—serum chemistry (week 4)[a]

Diet Treatment	NC[b] Vehicle	HFD[c] Vehicle	HFD[c] 10 mg/kg	HFD[c] 30 mg/kg	HFD[c] 100 mg/kg
Glucose (mg/dL)	296.9 ± 16.8	316.5 ± 13.2	313.0 ± 12.2	282.2 ± 10.4	241.4 ± 16.8[e]
Insulin (ng/mL)	0.49 ± 0.04	0.80 ± 0.12	0.63 ± 0.07	0.58 ± 0.07	0.34 ± 0.06[d]
TC[g] (mg/dL)	75.2 ± 3.3[f]	140.0 ± 2.8	108.5 ± 1.9[f]	99.6 ± 3.3[f]	87.9 ± 2.7[f]
TG[h] (mg/dL)	50.0 ± 1.3	54.4 ± 1.5	55.8 ± 2.5	51.1 ± 2.0	47.4 ± 4.0
NEFA[i] (mEq/dL)	0.42 ± 0.02	0.46 ± 0.02	0.53 ± 0.02	0.52 ± 0.02	0.65 ± 0.06[f]
Glycerol (mg/dL)	9.0 ± 0.7	11.0 ± 1.3	10.8 ± 0.8	10.0 ± 1.1	9.7 ± 0.7
β-HBA[j] (mg/dL)	1.8 ± 0.1	1.7 ± 0.1	1.7 ± 0.1	1.8 ± 0.1	3.3 ± 1.0[d]

[a] The results are presented as mean ± SEM and analyzed by one-way ANOVA followed by the Tukey's honest significance test. Serum samples were taken at the end of the study without fasting.
[b] NC = normal chow diet.
[c] HFD = high fat diet.
[d] p <0.05 versus the high fat diet group.
[e] p <0.01 versus the high fat diet group.
[f] p <0.001 versus the high fat diet group.
[g] TC = total cholesterol.
[h] TG = triglycerides.
[i] NEFA = non-esterified fatty acids.
[j] β-HBA = β-hydroxyybutyrate.

as the rodent toxicology species, during development of quinoline **1c**.

Since quinoline **1c** exhibited improved pharmacokinetics relative to GSK8062 **1b**, it was evaluated in a diet-induced obese (DIO) mouse model of diabetes. C57BL/6 J mice were fed with a high-fat diet for four weeks to establish obesity and insulin resistance, then randomized based on fasting glucose and body weight and assigned to different treatment groups. The mice were dosed by oral gavage for four weeks with the potassium salt of quinoline **1c** (mouse TT EC_{50} = 120 nM, %Max = 99) or vehicle, and subsequently sacrificed for analysis. The high fat diet increased body weight gain relative to a normal chow diet. As shown in Table 3, quinoline **1c** caused a dose-dependent decrease in body weight at 10, 30, and 100 mg/kg, mainly caused by a decrease in body fat mass (data not shown). Furthermore, the FXR agonist **1c** significantly and dose-dependently decreased serum glucose levels, relative to vehicle, with the maximum effect at 100 mg/kg (Table 4). This was accompanied by a decrease in serum insulin, which suggests a potential improvement in whole body insulin sensitivity. In addition, quinoline **1c** decreased triglycerides, total cholesterol, and glycerol, relative to the high fat diet controls.

In summary, a series of aza-naphthalene analogs of GSK8062 **1b** were synthesized as potential modulators of FXR. The quinoline **1c** was an equipotent full FXR agonist to GSK8062 **1b** with good selectivity versus related nuclear receptors. In addition, it was more water soluble and exhibited better rat pharmacokinetics than GSK8062 **1b**, possibly providing development advantages over GSK8062 **1b**. Furthermore, quinoline **1c** dose-dependently decreased serum glucose and body weight gain in the DIO mouse model. Thus, quinoline (GSK2324) **1c** may prove useful in further defining the physiological roles of FXR, as well as aiding the design of other FXR modulators.

Acknowledgement

The authors would like to thank Judi A. McNulty for assistance with the DIO mouse study.

Supplementary data

Supplementary data associated with this article can be found, in the online version, at doi:10.1016/j.bmcl.2010.12.089.

References and notes

1. Hylemon, P. B.; Zhou, H.; Pandak, W. M.; Ren, S.; Gil, G.; Dent, P. *J. Lipid Res.* **2009**, *50*, 1509.
2. Lefebvre, P.; Cariou, B.; Lien, F.; Kuipers, F.; Staels, B. *Physiol. Rev.* **2009**, *89*, 147.
3. Gupta, S.; Stravitz, R. T.; Dent, P.; Hylemon, P. B. *J. Biol. Chem.* **2001**, *276*, 15816.
4. Kawamata, Y.; Fujii, R.; Hosoya, M.; Harada, M.; Yoshida, H.; Miwa, M.; Fukusumi, S.; Habata, Y.; Itoh, T.; Shintani, Y.; Hinuma, S.; Fujisawa, Y.; Fujino, M. *J. Biol. Chem.* **2003**, *278*, 9435.
5. Eloranta, J. J.; Kullak-Ublick, G. A. *Physiology* **2008**, *23*, 286.
6. Forman, B. M.; Goode, E.; Chen, J.; Oro, A. E.; Bradley, D. J.; Perlmann, T.; Noonan, D. J.; Burka, L. T.; McMorris, T.; Lamph, W. W.; Evans, R. M.; Weinberger, C. *Cell* **1995**, *81*, 687.
7. Higashiyama, H.; Kinoshita, M.; Asano, S. *Acta Histochem.* **2008**, *110*, 86.
8. Lambert, G.; Amar, M. J. A.; Guo, G.; Brewer, H. B., Jr.; Gonzalez, F. J.; Sinal, C. J. *J. Biol. Chem.* **2003**, *278*, 2563.
9. Maloney, P. R.; Parks, D. J.; Haffner, C. D.; Fivush, A. M.; Chandra, G.; Plunket, K. D.; Creech, K. L.; Moore, L. B.; Wilson, J. G.; Lewis, M. C.; Jones, S. A.; Willson, T. M. *J. Med. Chem.* **2000**, *43*, 2971.
10. Watanabe, M.; Houten, S. M.; Wang, L.; Moschetta, A.; Mangelsdorf, D. J.; Heyman, R. A.; Moore, D. D.; Auwerx, J. *J. Clin. Invest.* **2004**, *113*, 1408.
11. Cariou, B.; van Harmelen, K.; Duran-Sandoval, D.; van Dijk, T.; Grefhorst, A.; Bouchaert, E.; Fruchart, J.-C.; Gonzalez, F. J.; Kuipers, F.; Staels, B. *FEBS Lett.* **2005**, *579*, 4076.
12. Ma, K.; Saha, P. K.; Chan, L.; Moore, D. D. *J. Clin. Invest.* **2006**, *116*, 1102.
13. Zhang, Y.; Lee, F. Y.; Barrera, G.; Lee, H.; Vales, C.; Gonzalez, F. J.; Willson, T. M.; Edwards, P. A. *Proc. Natl. Acad. Sci. U.S.A.* **2006**, *103*, 1006.
14. Inagaki, T.; Choi, M.; Moschetta, A.; Peng, L.; Cummins, C. L.; McDonald, J. G.; Luo, G.; Jones, S. A.; Goodwin, B.; Richardson, J. A.; Gerard, R. D.; Repa, J. J.; Mangelsdorf, D. J.; Kliewer, S. A. *Cell Metab.* **2005**, *2*, 217.
15. Inagaki, T.; Moschetta, A.; Lee, Y.-K.; Peng, L.; Zhao, G.; Downes, M.; Yu, R. T.; Shelton, J. M.; Richardson, J. A.; Repa, J. J.; Mangelsdorf, D. J.; Kliewer, S. A. *Proc. Natl. Acad. Sci. U.S.A.* **2006**, *103*, 3920.
16. Jung, D.; Inagaki, T.; Gerard, R. D.; Dawson, P. A.; Kliewer, S. A.; Mangelsdorf, D. J.; Moschetta, A. *J. Lipid Res.* **2007**, *48*, 2693.
17. Sonoda, J.; Rosenfeld, J. M.; Xu, L.; Evans, R. M.; Xie, W. *Curr. Drug Metab.* **2003**, *4*, 59.
18. Huang, W.; Ma, K.; Zhang, J.; Qatanani, M.; Cuvillier, J.; Liu, J.; Dong, B.; Huang, X.; Moore, D. D. *Science* **2006**, *312*, 233.
19. Fiorucci, S.; Clerici, C.; Antonelli, E.; Orlandi, S.; Goodwin, B.; Sadeghpour, B. M.; Sabatino, G.; Russo, G.; Castellani, D.; Willson, T. M.; Pruzanski, M.; Pellicciari, R.; Morelli, A. *J. Pharmacol. Exp. Ther.* **2005**, *313*, 604.
20. Liu, Y.; Binz, J.; Numerick, M. J.; Dennis, S.; Luo, G.; Desai, B.; MacKenzie, K. I.; Mansfield, T. A.; Kliewer, S. A.; Goodwin, B.; Jones, S. A. *J. Clin. Invest.* **2003**, *112*, 1678.
21. Stedman, C.; Liddle, C.; Coulter, S.; Sonoda, J.; Alvarez, J. G.; Evans, R. M.; Downes, M. *Proc. Natl. Acad. Sci. U.S.A.* **2006**, *103*, 11323.
22. Fiorucci, S.; Antonelli, E.; Rizzo, G.; Renga, B.; Mencarelli, A.; Riccardi, L.; Orlandi, S.; Pellicciari, R.; Morelli, A. *Gastroenterology* **2004**, *127*, 1497.
23. Fiorucci, S.; Rizzo, G.; Antonelli, E.; Renga, B.; Mencarelli, A.; Riccardi, L.; Morelli, A.; Pruzanski, M.; Pellicciari, R. *J. Pharmacol. Exp. Ther.* **2005**, *315*, 58.
24. Fiorucci, S.; Rizzo, G.; Antonelli, E.; Renga, B.; Mencarelli, A.; Riccardi, L.; Orlandi, S.; Pruzanski, M.; Morelli, A.; Pellicciari, R. *J. Pharmacol. Exp. Ther.* **2005**, *314*, 584.
25. Zhang, S.; Wang, J.; Liu, Q.; Harnish, D. C. *J. Hepatol.* **2009**, *51*, 380.
26. Kim, I.; Morimura, K.; Shah, Y.; Yang, Q.; Ward, J. M.; Gonzalez, F. J. *Carcinogenesis* **2007**, *28*, 940.
27. Yang, F.; Huang, X.; Yi, T.; Yen, Y.; Moore, D. D.; Huang, W. *Cancer Res.* **2007**, *67*, 863.
28. Cariou, B. *Diabetes Metab.* **2008**, *34*, 685.
29. Evans, M. J.; Mahaney, P. E.; Borges-Marcucci, L.; Lai, K.; Wang, S.; Krueger, J. A.; Gardell, S. J.; Huard, C.; Martinez, R.; Vlasuk, G. P.; Harnish, D. C. *Am. J. Physiol.* **2009**, *296*, G543.
30. Hanniman, E. A.; Lambert, G.; McCarthy, T. C.; Sinal, C. J. *J. Lipid Res.* **2005**, *46*, 2595.
31. Hartman, H. B.; Gardell, S. J.; Petucci, C. J.; Wang, S.; Krueger, J. A.; Evans, M. J. *J. Lipid Res.* **2009**, *50*, 1090.
32. Zhang, Y.; Wang, X.; Vales, C.; Lee, F. Y.; Lee, H.; Lusis, A. J.; Edwards, P. A. *Arterioscler., Thromb., Vasc. Biol.* **2006**, *26*, 2316.
33. Moschetta, A.; Bookout, A. L.; Mangelsdorf, D. J. *Nat. Med.* **2004**, *10*, 1352.
34. Hansen, M. K.; Connolly, T. M. *Curr. Opin. Invest. Drugs* **2008**, *9*, 247.
35. Cariou, B.; Staels, B. *Trends Pharmacol. Sci.* **2007**, *28*, 236.
36. Abel, U.; Schlueter, T.; Schulz, A.; Hambruch, E.; Steeneck, C.; Hornberger, M.; Hoffmann, T.; Perovic-Ottstadt, S.; Kinzel, O.; Burnet, M.; Deuschle, U.; Kremoser, C. *Bioorg. Med. Chem. Lett.* **2010**, *20*, 4911.
37. Akwabi-Ameyaw, A.; Bass, J. Y.; Caldwell, R. D.; Caravella, J. A.; Chen, L.; Creech, K. L.; Deaton, D. N.; Jones, S. A.; Kaldor, I.; Liu, Y.; Madauss, K. P.; Marr, H. B.; McFadyen, R. B.; Miller, A. B.; Navas, F., III; Parks, D. J.; Spearing, P. K.; Todd, D.; Williams, S. P.; Wisely, G. B. *Bioorg. Med. Chem. Lett.* **2008**, *18*, 4339.
38. Akwabi-Ameyaw, A.; Bass, J. Y.; Caldwell, R. D.; Caravella, J. A.; Chen, L.; Creech, K. L.; Deaton, D. N.; Madauss, K. P.; Marr, H. B.; McFadyen, R. B.; Miller, A. B.; Navas, F.; Parks, D. J.; Spearing, P. K.; Todd, D.; Williams, S. P.; Wisely, G. B. *Bioorg. Med. Chem. Lett.* **2009**, *19*, 4733.
39. Bass, J. Y.; Caldwell, R. D.; Caravella, J. A.; Chen, L.; Creech, K. L.; Deaton, D. N.; Madauss, K. P.; Marr, H. B.; McFadyen, R. B.; Miller, A. B.; Parks, D. J.; Todd, D.; Williams, S. P.; Wisely, G. B. *Bioorg. Med. Chem. Lett.* **2009**, *19*, 2969.
40. Feng, S.; Yang, M.; Zhang, Z.; Wang, Z.; Hong, D.; Richter, H.; Benson, G. M.; Bleicher, K.; Grether, U.; Martin, R. E.; Plancher, J.-M.; Kuhn, B.; Rudolph, M. G.; Chen, L. *Bioorg. Med. Chem. Lett.* **2009**, *19*, 2595.
41. Pellicciari, R.; Fiorucci, S.; Camaioni, E.; Clerici, C.; Costantino, G.; Maloney, P. R.; Morelli, A.; Parks, D. J.; Willson, T. M. *J. Med. Chem.* **2002**, *45*, 3569.
42. Downes, M.; Verdecia, M. A.; Roecker, A. J.; Hughes, R.; Hogenesch, J. B.; Kast-Woelbern, H. R.; Bowman, M. E.; Ferrer, J.-L.; Anisfeld, A. M.; Edwards, P. A.; Rosenfeld, J. M.; Alvarez, J. G. A.; Noel, J. P.; Nicolaou, K. C.; Evans, R. M. *Mol. Cell* **2003**, *11*, 1079.
43. Flatt, B.; Martin, R.; Wang, T.-L.; Mahaney, P.; Murphy, B.; Gu, X.-H.; Foster, P.; Li, J.; Pircher, P.; Petrowski, M.; Schulman, I.; Westin, S.; Wrobel, J.; Yan, G.; Bischoff, E.; Daige, C.; Mohan, R. *J. Med. Chem.* **2009**, *52*, 904.
44. Bass III, J. Y.; Deaton, D. N.; Caravella, J.; McFadyen, R. B.; Navas, F.; Spearing, P. K. PCT Int. Appl. WO 096921, 2008; *Chem. Abstr.* **2008**, *148*, 472019.
45. Chan, G.; Johns, A.; Jurewicz, A.; Porter, R. A.; Widdowson, K. PCT Int. Appl. WO 09024, **1999**; Chan, G.; Johns, A.; Jurewicz, A.; Porter, R. A.; Widdowson, K. *Chem. Abstr.* **1999**, *130*, 196581.
46. Buchstaller, H.-P.; Burgdorf, L.; Finsinger, D.; Amendt, C.; Grell, M.; Sirrenberg, C.; Zenke, F. PCT Int. Appl. WO 082858, 2005; *Chem. Abstr.* **2005**, *143*, 286297.
47. Irvine, J. D.; Takahashi, L.; Lockhart, K.; Cheong, J.; Tolan, J. W.; Selick, H. E.; Grove, J. R. *J. Pharm. Sci.* **1999**, *88*, 28.